Heterotrimeric kinesin-II is necessary and sufficient to promote different stepwise assembly of morphologically distinct bipartite cilia in *Drosophila* antenna

Swadhin C. Jana, Mukul Girotra, and Krishanu Ray
Tata Institute of Fundamental Research, Colaba, Mumbai 400005, India

ABSTRACT **Structurally diverse sensory cilia have evolved from primary cilia, a microtubule-based cellular extension engaged in chemical and mechanical sensing and signal integration. The diversity is often associated with functional specialization. The olfactory receptor neurons in *Drosophila*, for example, express three distinct bipartite cilia displaying different sets of olfactory receptors on them. Molecular description underlying their assembly and diversification is still incomplete. Here, we show that the branched and the slender olfactory cilia develop in two distinct step-wise patterns through the pupal stages before the expression of olfactory receptor genes in olfactory neurons. The process initiates with a thin procilium growth from the dendrite apex, followed by volume increment in successive stages. Mutations in the kinesin-II subunit genes either eliminate or restrict the cilia growth as well as tubulin entry into the developing cilia. Together with previous results, our results here suggest that heterotrimeric kinesin-II is the primary motor engaged in all type-I sensory cilia assembly in *Drosophila* and that the cilia structure diversity is achieved through additional transports supported by the motor during development.**

Monitoring Editor
Monica Bettencourt-Dias
Instituto Gulbenkian de Ciência

Received: Aug 23, 2010
Revised: Dec 30, 2010
Accepted: Jan 5, 2011

INTRODUCTION

Sensory neurons grow cilia of varying morphology and function from the tips of their respective dendrites. Many of these cilia consist of a doublet microtubule (MT)-bearing proximal/middle segment and a distal/outer part containing combinations of singlet MTs (Reese, 1965; Shanbhag *et al.*, 1999), actin filaments (Arikawa and Williams, 1989; Chaitin, 1991), and membranous folds (Ward *et al.*, 1975) (reviewed in Silverman and Leroux, 2009). The tube-like middle segment often contains a 9+0 axoneme as found in the primary cilia. The outer parts are highly divergent in morphology and composition and display the sensory receptors. Sensory cilia evolved from an essential cellular appendage called primary cilium (Davenport and Yoder, 2005). The latter is involved in sensing the chemical (Singla and Reiter, 2006) and mechanical stimuli (Praetorius and Spring, 2001; Jaffe, 2007), signal integration during development (Corbit *et al.*, 2005; Chizhikov *et al.*, 2007; Goetz and Anderson, 2010) and in many other functions (Hirokawa *et al.*, 2006). Dysfunctional cilia cause physical disorders, such as polycystic kidney disease (Yoder *et al.*, 2002; Davenport *et al.*, 2007), Bardet-Biedle syndrome (BBS) (Loktev *et al.*, 2008; Shah *et al.*, 2008), and cancer (Wong *et al.*, 2009). Therefore, understanding mechanisms underlying the cilia assembly and diversification has significant implications.

Anterograde intraflagellar transport (IFT) (Kozminski *et al.*, 1995) powered by the heterotrimeric motors of the kinesin-2 family (Cole *et al.*, 1993) assembles as well as maintains the flagella and primary cilia (Scholey, 2003; Pedersen *et al.*, 2006). Kinesin-II subunits are also involved in maintaining the chordotonal cilia–bearing 9+0 axoneme on Johnston's organ neurons in *Drosophila* (Sarpal *et al.*, 2003). Meticulous analysis in *Caenorhabditis elegans*, however, revealed that kinesin-II plays a redundant role in the maintenance of the bipartite channel cilia on ASH/ASI neurons (Snow *et al.*, 2004).

This article was published online ahead of print in MBoC in Press (http://www.molbiolcell.org/cgi/doi/10.1091/mbc.E10-08-0712) on January 13, 2011.

Address correspondence to: Krishanu Ray (krishanu@tifr.res.in).

Abbreviations used: APF, after pupa formation; BBS, Bardet-Biedle syndrome; CC, connecting cilium/a; DmKAP, *Drosophila melanogaster* kinesin–associated protein (KAP3A orthologue); EAG, electroantennogram; eGFP, enhanced green fluorescent protein; IFT, intraflagellar transport; IS, inner segment; KIF17, kinesin-family protein 17 (Osm-3 orthologue); KLP64D, kinesin-like protein 64D (Kif3A orthologue); KLP68D, kinesin-like protein 68D (homologues to both Kif3B and 3C); MT, microtubule; OR, olfactory receptor; ORN, olfactory receptor neuron; OS, outer segmentl Osm-3, osmotic avoidance abnormal-3 (homodimeric kinesin-2 family motor); TEM, transmission electron micrographs; UAS, upstream activation sequence; YFP, yellow fluorescent protein.

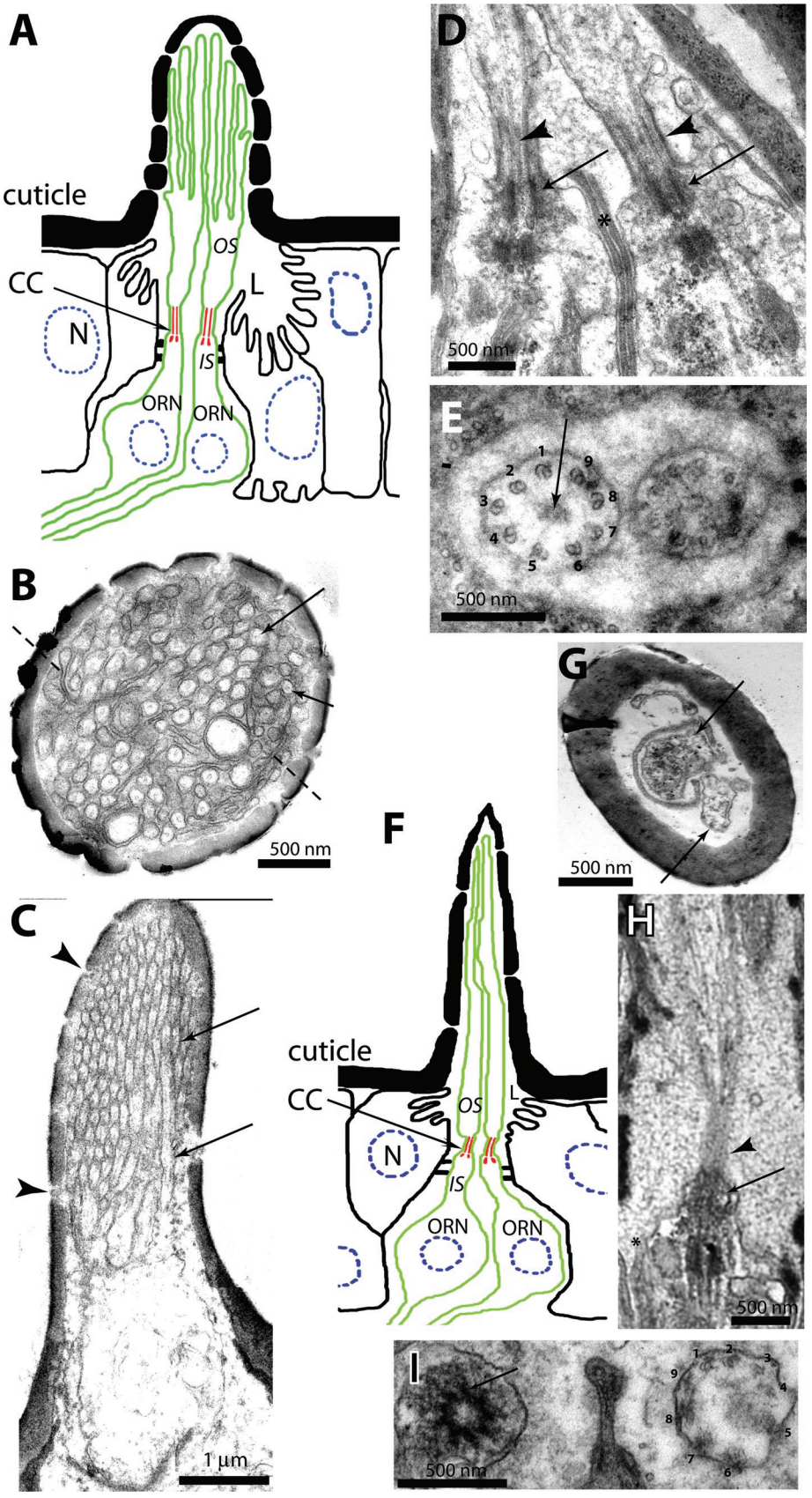

FIGURE 1: Anatomy of olfactory cilium expressed on the neurons innervating *s. basiconica* and *s. trichodea*. (A) Schematic illustrates the cellular organization of an *s. basiconicum*. L, receptor lymph. (B–E) Transmission electron micrographs (TEMs) of sections through *s. basiconica* with scale bars as indicated on each figure. (B) A cross-section view through the middle of a sensillum shaft. Arrows indicate the branches containing singlet MT, and dashed lines indicate the membranous lamellae devoid of MT. (C) An oblique section of the sensillum shaft shows tightly packed OS branches (arrows) and structures of the small cuticular pores (arrowheads). (D) A longitudinal section through the olfactory cilia of two ORNs shows the distal basal bodies (arrows), the axonemes (arrowheads), and the sheath cell junctions (asterisk). (E) A cross section through the cilia base shows radial arrangement of nine doublet MTs (marked with numerals 1–9) with some electron-dense material (arrow) at the central region in each CC. The sheath cell extensions encapsulate the cilia at their base as depicted in this figure. (F) Schematic illustrates the cellular organization of a *s. trichodium*. (G–I) TEMs of sections through *s. trichodea* with scale bars as indicated on each figure. (G) A cross-section view through the middle of a sensillum shaft. Arrows mark two distinct OSs, and dashed lines indicate the membranous lamellae devoid of MT. (H) A longitudinal section through an olfactory cilium shows the distal basal body (arrow) and the axoneme (arrowhead). (I) A cross section through the cilia base shows radial arrangement of nine doublet MTs (marked with numerals 1–9). The pictures presented in the figure are for reference. The MTs in the OSs of ORNs are better preserved when the antennae are fixed by the high-pressure freeze substitution method as shown earlier by Shanbhag *et al.* (1999).

The anterograde IFT in the ASH/ASI cilia is jointly propelled by heterotrimeric Cekinesin-II and homodimeric (Osm-3) motors in the middle segment, and it is supported by the Osm-3 alone in the distal segments (Snow *et al.*, 2004). The switch is coordinated by the BBS7/8 complex and Dyf-1 (Ou *et al.*, 2005; Pan *et al.*, 2006). This evidence helped to introduce the concepts of "canonical" and "accessory" IFT motors being used to generate the additional cilia diversity (Evans *et al.*, 2006), and defined operations of a complex motor function-coordination system (Pan *et al.*, 2006). A comparable motor function organization was reported in the vertebrate photoreceptor cells where kinesin-family protein 17 (KIF17), an Osm-3 orthologue, is shown to play a key role in the rod outer segment assembly (Insinna *et al.*, 2008). In contrast, KIF17 was found to play a minor role in the primary cilia where it is engaged in transporting sensory receptors (Jenkins *et al.*, 2006). Studies in *C. elegans* further revealed that the functioning and plasticity of the distal segments of the odor-receptive cilia on AWB and the AWC neurons depends on kinesin-II alone (Evans *et al.*, 2006; Mukhopadhyay *et al.*, 2007). Furthermore,

kinesin-II was reported to be the motor responsible for membrane delivery to the outer segment of cone photoreceptors in mice (Avasthi *et al.*, 2009). Although these results established that separate kinesin-II–mediated transports are associated with the cilia diversification, several critical issues concerning the cilia assembly and initiation of the process remained unanswered.

The olfactory receptor neurons (ORNs) in *Drosophila* antennae express three morphologically distinct cilia displaying different sets of olfactory receptors (ORs) (van der Goes van Naters and Carlson, 2007). These morphologically distinct cilia offer an excellent model for a comparative study of the basic cilia assembly and diversification mechanisms. Here, we present the results of a systematic investigation of the growth patterns of two morphologically distinct olfactory cilia and the role of heterotrimeric kinesin-II in the process. Our results suggest that different stepwise transport strategies are used to develop morphologically distinct cilia. In addition, heterotrimeric kinesin-II–dependent tubulin entry plays a crucial role in the ciliary axoneme assembly and growth at each stage.

RESULTS

Adult *Drosophila* antenna contains three morphologically distinct *sensilla*, each innervated with two to four ORNs (Shanbhag *et al.*, 1999). Each ORN type extends a morphologically distinct bipartite cilium from the basal bodies at the distal end of the dendritic inner segment (IS) into the hollow cuticular shaft. The outer segments (OSs) of the cilia found on ORNs innervating *sensilla basiconica*, for instance, have several branches each containing up to three singlet MT filaments (Figure 1, A–C). The OS grows from a ~1-μm-long connecting cilium (CC) in the middle (Figure 1D), which contains 9+0 axoneme (Figure 1E). The MT organization in the cilia extended from the ORNs innervating *sensilla trichodea* (Figure 1F), however, resembles the ASH/ASI cilia of *C. elegans* (Evans *et al.*, 2006). It contains a long slender OS-bearing multiple singlet MTs, which grows from a compact CC (>0.5 μm) consisting of a 9+0 axoneme (Figure 1, G–I). The *s. coeloconica*, in contrast, are typically innervated with two ORNs expressing relatively shorter cilia bearing multiple singlet MTs (Shanbhag *et al.*, 1999). ORs expressed in an ORN determine its odor specificity (Dobritsa *et al.*, 2003), and all ORs are transported into the OS in an OR83b-dependent manner (Larsson *et al.*, 2004; Benton *et al.*, 2006), which is essential for odor receptions. Little is known about the cilia growth and the mechanism determining its structural diversification.

Olfactory cilia grow in discrete steps during the pupal stages

Therefore, we studied cilia growth from ORNs innervating specific *s. basiconica* and *s. trichodea*, whose positions are reliably distinguishable on the developing antenna. The ORNs innervating *s. basiconica* of anatomical type LB-II1/2 (Shanbhag *et al.*, 1999), and the functional type ab2/3 (Clyne *et al.*, 1997; de Bruyne *et al.*, 2001), and the T3 type *s. trichodea* (Shanbhag *et al.*, 1999) were selected for this purpose. The reporter gene expressions in the enhanced green fluorescent protein (*UAS-eGFP*) $Gal4^{SG18.1}$ (Figure 2, A and B), as well as in the *UAS-eGFP* $Gal4^{cha19b}$ (Supplemental Figure 1) stocks marked the ORNs in the developing antenna from 30 to 100 h after pupa formation (APF). Image analysis of the growing ORNs revealed that the cilia on the ORNs, innervating both *s. basiconica* and *s. trichodea* (hereafter termed basiconic and trichoid cilia, respectively), start growing between 30 and 36 h APF and they are fully extended by 100 h APF (Figure 2, A and B). At 72 h APF, the eGFP marking was less pronounced in the proximal portion of the basiconic cilia (highlighted by paired dotted lines, Figure 2A-d) as compared with the distal parts (arrowheads, Figure 2A-d). The brightness and width of the distal parts continued to grow in subsequent stages (arrowhead, Figure 2A-e). Thus, the proximal portion came to resemble the CC, and the distal portion the OS from this stage. The trichoid cilia, however, extended up to 90% of the final length by 72 h APF (arrowhead, Figure 2B-d) and mostly increase in width after that. Image quantification also revealed that the volume and length of the developing basiconic cilia progressively increased between 36 and 72 h and between 84 and 96 h (Figure 2C-a) interspersed by a short (6 h) stationary phase, whereas both occur in a single phase between 36 and 90 h for the trichoid cilia (Figure 2C-b). Together, the cilia length and volume analyses showed that morphologically distinct olfactory cilia grow in different patterns. It is to be noted that the OR gene expression in the neurons starts at 90 h APF and that fly antenna starts responding to odors a few hours after eclosion (Larsson *et al.*, 2004). Therefore, our observation would suggest that morphology of olfactory cilia is determined independent of sensory inputs.

The 10- to 15-μm-long *Chlamydomonas* flagella were reported to regenerate in 2 h at 0.2–0.4 μm/min (Lefebvre *et al.*, 1978; Lefebvre and Rosenbaum, 1986). Although the growth profile of trichoid cilia matched well with that of the flagella regeneration profiles observed earlier (Lefebvre and Rosenbaum, 1986), it occurs at a rate that is far too slow. An intermediate rate of cilia growth (0.035–0.065 μm/min) was measured in sea urchin embryos (Burns, 1979). Both the motile cilia and flagella, however, contain 9+2 doublet MT-bearing axoneme, which is significantly different from the bipartite axoneme organization in the olfactory cilia. These morphological differences could account for the observed slow growth of the olfactory cilia. The biphasic growth observed for the basiconic cilia is, however, a novel observation. This type of growth may require the induction of a second phase of transport into the cilia for growing the singlet branches. *Chlamydomonas* also extends singlet MT-bearing projections from the flagellar tip for a brief period during mating, which is involved in pheromone sensing and flagella adhesion (Mesland *et al.*, 1980). Both heterotrimeric kinesin-II (Pan and Snell, 2002), as well as IFT (Wang *et al.*, 2006), are implicated in this process.

Loss of kinesin-II function in ORNs affects olfactory reception at the adult antenna

Kinesin-II motor subunit homologues kinesin-like protein 64D (KLP64D) and kinesin-like protein 68D (KLP68D) form a heterotrimeric complex with *Drosophila melanogaster* kinesin–associated protein (DmKAP) in *Drosophila* (Doodhi *et al.*, 2009). Loss of function mutations in the *Klp64D* and the *DmKap* was shown to affect the sound-evoked electrical responses and eliminate the 9+0 axoneme-bearing sensory cilia of chordotonal neurons (Sarpal *et al.*, 2003). The role of KLP68D in the process is yet to be tested. Hence, to identify their roles in olfactory cilia assembly and maintenance, we screened individual kinesin-II subunit mutants for olfaction defects using the odor-evoked electroantennogram (EAG) assay (Alcorta, 1991), because any defect in cilia growth and maintenance would affect the odor reception.

We found that the EAG responses were significantly reduced from the homozygous $Klp64D^{k5/k5}$ and several other transallelic mutant ($Klp64D^{k1/k5}$, $Klp64D^{l4/k5}$, and $Klp64D^{l4/k1}$) combinations (Figure 3B). The phenotypes were recessive and rescued by the ectopic expressions of two different recombinant *KLP64D* transgenes in the mutant backgrounds (Figure 3B). The genetic complementation and rescue experiments established that the EAG defects map to

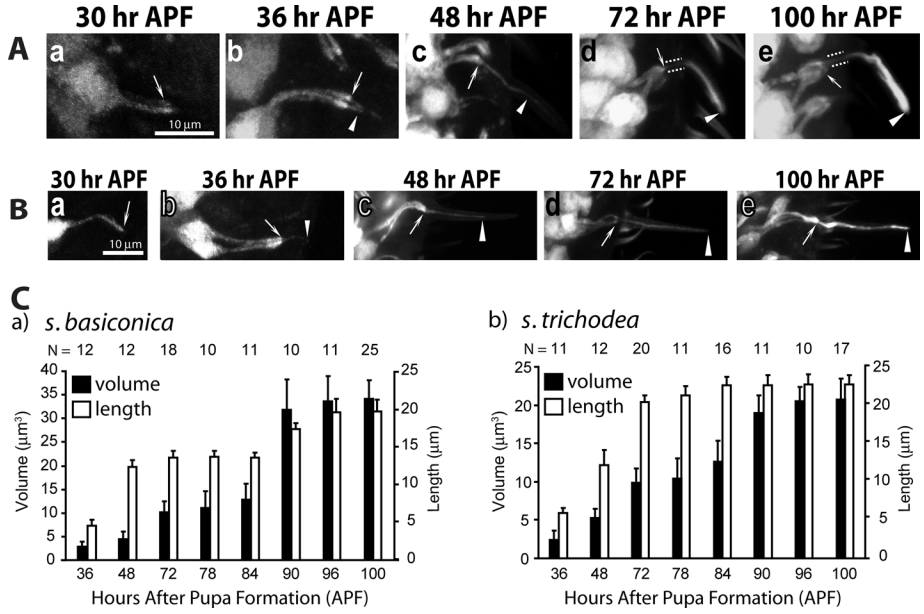

FIGURE 2: Analysis of the olfactory cilia growth in the pupal antennae. (A and B) Stages of olfactory cilia growth on ORNs innervating *s. basiconica* (A) and *s. trichodea* (B) in the developing antennae. *UAS-eGFP* expression in the ORNs due to *Gal4*$^{SG18.1}$ marked the ORNs and all its extensions including the cilia from an early stage of development. Arrows indicate the cilia base at the IS apex, paired dotted lines indicate the CC region, and the arrowhead indicates the OS in each panel. Scale bar = 10 µm for all panels. (C) Histograms depict the growth of the cilia volume and lengths inside *s. basiconica* (a) and *s. trichodea* (b) shafts in developing wild-type antennae. Error bars indicate ± standard deviation, and the sample size (N values) is indicated on top of each bar.

the *Klp64D* locus. The rescue due to the expressions of *UAS-KLP64D:GFP* by *Gal4*$^{SG18.1}$ or *Gal4*^{chat19b} (Figure 3B) further suggested that the *Klp64D* gene function is required in the ORNs. Similar reductions in the EAG responses were caused by two different P-element insertions in the *Klp68D* upstream, which is rescued by the *UAS-KLP68D:*yellow fluorescent protein (*YFP*) expression in the background (Figure 3C). The transgenic rescue experiment implicated KLP68D in the odor reception process. Finally, mutations in *DmKap* are found to eliminate the EAG responses, and they were restored due to the presence of the genomic transgene as well as *Gal4*$^{SG18.1}$-mediated *UAS-DmKap* expression in the mutant background (Figure 3D). Both the *DmKap* alleles (*v5* and *v6*) were documented as genetic null earlier (Sarpal *et al.*, 2003), which is further confirmed by the EAG measurements. In comparison, the *Klp64D* and *Klp68D* alleles used for the screen appeared to be hypomorphic. Together, the EAG analysis implicated all three kinesin-II subunits in the maintenance of odor reception by ORNs.

Kinesin-II subunits are essential for maintaining the basiconic and trichoid cilia

Therefore, to understand the cellular basis of the EAG defects observed in the kinesin-II mutants, we studied the anatomy of the basiconic and trichoid cilia in the wild-type and mutant antennae obtained from pharate adults (100 h APF). The *UAS-eGFP* expression due to *Gal4*$^{SG18.1}$ revealed that the ISs are extended from almost all ORNs in the *Klp64D, Klp68D*, and *DmKap* mutant antennae (arrows, Figure 4A). Nearly 90% of the ORNs in the *Klp64D*^{k1} antenna, however, expressed visibly thin cilia (arrowhead, Figure 4A; Table 1), and the others did not have any cilia (open arrowhead, Figure 4). These morphological defects were fully rescued by ectopic expression of the recombinant *Klp64D* transgene in the ORNs (arrowhead, Figure 4A). Almost 98% of ORNs in *Klp68D*^{KG03849} homozygous antennae expressed cilia (Figure 4, A-d and I; Table 1). Many of these cilia were comparatively brighter and healthier than the ones observed in the *Klp64D* mutants. The average volume of individual cilia was reduced to below 50% of wild-type values in the *Klp64D*^{k1} and to almost 65% of wild-type in the Klp68D^{KG03849} homozygous backgrounds (Figure 4B). The variations, however, were large in the *Klp68D* background, which suggests that mutation in *Klp68D* has incomplete penetrance. In contrast, cilia were absent on nearly 80% of the ORNs in the *DmKap*^{v6} homozygous antennae (Table 1). The cilia defects were most severe in the *DmKap*^{v6} background, which is known to be a null allele, and qualitatively more severe in *Klp64D*^{k1} than in the *Klp68D*^{KG30849} homozygous antennae. In addition, we found that the gustatory cilia inside labellar hairs were eliminated in *DmKap*^{v6} mutants (Supplemental Figure 3), and an earlier study reported the total loss of chordotonal cilia on neurons innervating the Johnston's organ in the second antennal segment (Sarpal *et al.*, 2003).

TEM electron micrograph study of the 1-d-old *Klp64D* mutant adults showed that often the electron-dense basal bodies and the CC are present at the dendrite tips of the ORNs (Figure 4C), but the number of OS branches of the basiconic cilia was either reduced or fused (Figure 4C). The phenotype manifested in a qualitatively different manner in the homozygous *Klp64D*^{k5} (Figure 4C-a) as compared with the *Klp64D*$^{l4/k5}$ (Figure 4C-b) backgrounds. The OS of basiconic cilia are less branched in the *Klp64D*^{k5} homozygous antennae as compared to the wild-type (Figure 4D), whereas the OS in the *Klp64D*$^{l4/k5}$ antennae usually contained a slender extension with several singlet MTs (Figure 4E). These suggested that *Klp64D* gene function is essential for OS branching and MT organization in these branches. The diversity of the anatomical phenotypes in different *Klp64D* alleles also indicates that the gene function is involved in different ciliary processes. Several attempts to obtain a properly fixed *Klp64D*^{k1} homozygous antenna failed as we mostly found degenerated tissue inside. In contrast, entire cilia, including the junctions between the IS and the sheath cells, were

	Wild-type	*Klp64D*^{k1}	*Klp64D*$^{l4/k1}$	*Klp68D*^{KG03849}	*DmKap*^{v6}
% Basiconic cilia	100 (116/116)	95.6 (44/46)	98.3 (60/61)	98.5 (65/66)	8 (8/101)
% Tricoidic cilia	100 (85/85)	88 (30/34)	88.9 (40/45)	96.1 (49/51)	16.4 (10/57)

TABLE 1: Relative abundance of cilia inside *s. basiconica* and *s. trichodea* shafts in wild-type and kinesin-II subunit mutant antennae.

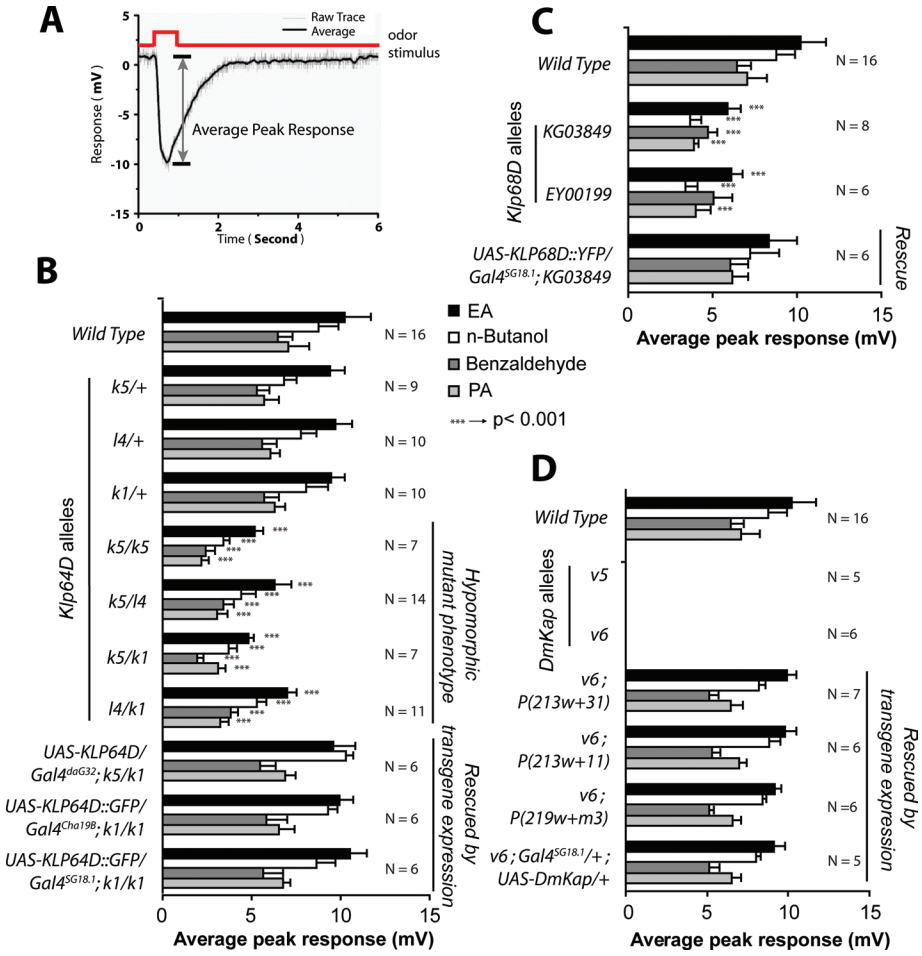

FIGURE 3: Odor-evoked potential changes in the wild type and kinesin-II mutant antennae. (A) Typical odor-evoked potential response measured from the wild-type adult antenna. The maximum potential difference (arrow) from the base line (set at 0) is measured as the EAG response to an odor pulse. (B) Histograms indicate EAG responses measured from the third antennal segments of wild-type controls, different *Klp64D* alleles, and transgenic rescue stocks in response to ethyl acetate (EA, solid filled bars), n-butanol (open bars), benzaldehyde (gray filled bars), and propionic acid (PA, light gray bars). Error bars indicate ± standard deviation, and the corresponding sample sizes (N values) are indicated on the right margin. (C and D) Similar EAG measurements were made in the homozygous *Klp68D* mutants and transgenic rescue stocks (C) as well as from the antennae of the *DmKap* homozygous mutant adults (D). Although the latter does not respond to any odor, the defect is fully restored by transgenic *DmKap* expression in the olfactory neurons (D). The pair-wise significance of the difference between the appropriate pair of wild-type and mutant data is tested by Student's *t* test, and highly significant differences ($p < 0.001$) are depicted by *** on the bars.

absent in the *DmKap*^{v6} antennae (Figure 4F). A similar study using the available *Klp68D*^{KG03849} remained inconclusive due to incomplete and variable penetrance of the cilia phenotype within a single antenna. The anatomical defects observed are consistent with the corresponding decrease in EAG responses. For instance, a lower number of branches, as seen in the *Klp64D* mutant antennae, is expected to reduce the overall surface area and the net electrical impedance of the OS, thus lowering the overall potential change on odor stimulation as depicted in the EAG records from *Klp64D* and *Klp68D* mutants. Similarly, a total loss of cilia in the *DmKap* mutants was found to eliminate the EAG response. Together with the optical microscopy data, these results indicated that the heterotrimeric kinesin-II consisting of DmKAP, KLP64D, and KLP68D plays prominent roles in the olfactory cilia formation or maintenance.

The heterotrimeric kinesin-II subunits are shown to move independently of Osm-3 into the distal segments of the AWB (Mukhopadhyay *et al.*, 2007) and the AWC cilia (Evans *et al.*, 2006) in *C. elegans*. It was also reported that Osm-3 and kinesin-II are redundant for cilia length extensions, but functioning of the mature AWC cilia depends on kinesin-II (Evans *et al.*, 2006). The data presented here suggest that the kinesin-II subunits are involved in the OS assembly in olfactory cilia like Osm-3 in the distal segments of ASH/ASI cilia in *C. elegans* (Snow *et al.*, 2004) and KIF17 in the OSs of rod photoreceptors (Insinna *et al.*, 2008).

Mutations in Klp64D and DmKap affect the initiation of olfactory cilia assembly

To assess the roles of kinesin-II subunits during the olfactory cilia assembly, we studied the ciliary growth in *Klp64D*^{k1} and *DmKap*^{v6} homozygous antennae. Growth showed that, although the cilia length extension was marginally reduced until 72 h APF (Figure 5, A and B), the length and volume expansions of both the basiconic and trichoid cilia at the second stage were significantly reduced in the *Klp64D* mutants (Figure 5, C and D). This observation established a KLP64D requirement in the second stage of cilia growth, which involves OS branching in basiconic cilia and volume increment in trichoid cilia. In addition, 6–7% of the ORNs in *Klp64D*^{k1} antenna failed to grow cilia from the beginning, indicating that the gene function is also necessary for initiating the cilia growth. Interestingly, a similar two-stage cilia growth defect was observed in sea urchin embryos where injection of a Sp-KRP85 (Kif3A and KLP64D homologue) specific monoclonal antibody inhibited cilia growth after the initiation of an immotile short cilium containing 9+0 axoneme (Morris and Scholey, 1997). Furthermore, we found that the ciliary extensions did not grow from a majority of ORNs in the *DmKap* mutants (Supplemental Figure 2), suggesting that, in addition to KLP64D, DmKAP is also needed for inducing the cilia growth.

Therefore, light microscopy and TEM characterizations of the adult cilia in wild type and *Klp64D* mutants and the developmental defects determined in *Klp64D* mutants suggest that a thin procilium, containing 9+0 axoneme in the CC and a slender OS, would initially grow from the IS tip. The initiation of cilia growth would require DmKAP and KLP64D. Further KLP64D-dependent transport then augments this growth, which manifests as branching or volume increments of OS in certain cases. The difference in the severity and penetrance of the early growth defects observed in the *Klp64D* and *DmKap* mutants is consistent in both the EAG and cellular characterization data. This is possibly caused by the

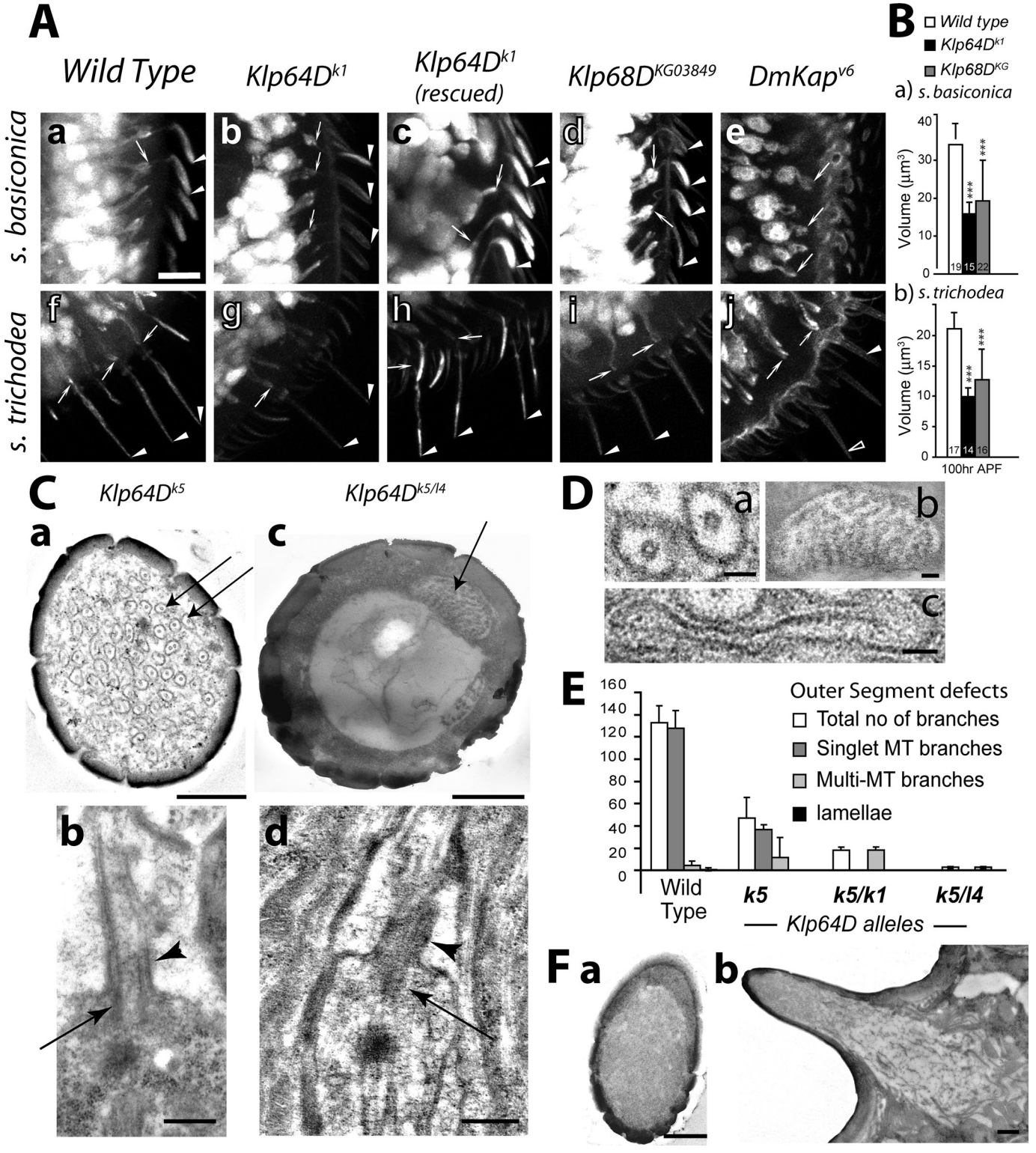

FIGURE 4: Anatomy of the olfactory cilia in the homozygous *Klp64D*, *Klp68D*, and *DmKap* mutant antennae. (A) *UAS-eGFP* expression in the ORNs due to *Gal4*$^{SG18.1}$ marked the entire cell including the cilia inside *s. basiconica* (a–e) and *s. trichodea* (f–j) shafts in the wild type (a and f), homozygous *Klp64D*^{k1} (b and g), *UAS-KLP64D*; *Klp64D*$^{k1/k1}$ (c and h), *Klp68D*^{KG} (d and i), and *DmKap*^{v6} antennae. Arrow indicates the cilia base in IS, and the arrowheads indicate the cilia OS; open arrowheads indicate empty shaft. Scale bar = 10 µm for all figures. (B) Histograms indicate the average cilia volumes in wild-type, *Klp64D*^{k1}, and *Klp68D*^{KG03849} homozygous mutant antennae. The error bars indicate ± standard deviation, and highly significant differences (***; $p < 0.001$) are depicted on the bars. (C) TEM images of sections through the sensory shafts of *s. basiconica* form homozygous *Klp64D*^{k5} (a and b) and *Klp64D*$^{k5/l4}$ (c and d) antennae. Arrows indicate the OS branches containing singlet MTs in (a) and multiple MTs in (c). Oblique sections through the basiconic cilia in *Klp64D*^{k5} (b) and *Klp64D*$^{k5/l4}$ (d) antennae showed the presence of basal bodies (arrows) and CC (arrowheads). (D) Magnified views of different types of branch morphologies found in *s. basiconica* shafts from

	UAS-KLP64D:GFP Gal4^{cha19b}/+			UAS-KLP68D:YFP Gal4^{cha19b}/+	
Genotype	***DmKap^{v6}/+***	***DmKap^{v6}/Y***	***DmKap^{v5}/Y***	***DmKap^{v6}/+***	***DmKap^{v6}/Y***
% Basiconic cilia	100 (66/66)	76.5 (62/81)	65 (37/57)	96.3 (52/54)	19.5 (8/41)
% Tricoidic cilia	100 (47/47)	73.4 (17/23)	72 (18/25)	100 (45/45)	32 (8/25)

TABLE 2: Relative abundance of basiconic and trichoid cilia growth due to ectopic expression of *UAS-KLP64D:GFP* and *UAS-KLP68D:YFP* in ORNs in wild-type and *DmKap* mutant backgrounds.

difference in the allelic natures of the two mutants. Alternatively, one can interpret the same results by suggesting that KLP64D plays a minor role at the beginning while a hitherto unknown DmKAP-containing motor would initiate the cilia growth.

KLP64D localizes to the cilia throughout development, and its overexpression initiates cilia extension in the absence of *DmKap*

To test whether KLP64D function would be necessary for the initiation of the procilium growth, we first studied the KLP64D:GFP localization into the olfactory cilia during development. Ectopic expression of *UAS-KLP64D:GFP* in the ORNs in *Gal4^{cha19b}* background labeled the growing basiconic and trichoid cilia from 36-h APF (Figure 6, A and E). The localization in the cilia grew along with the length increment in successive stages (Figure 6, B–D and F–H). The fusion protein was also enriched at the cilia base at 36 h APF (Figure 6, A and E), and the intensity of the localization progressively increased from 36 to 100 h APF, indicating that the kinesin-II is actively transported into the OS during these stages. The entry of kinesin-II is further confirmed by measuring the lengths and volume of the cilia highlighted by KLP64D:GFP, which produced an almost identical pattern to that observed with the GFP localizations earlier (Figure 6, I and J). This result indicated that KLP64D could enter the cilia from the initial stage of development. Once again, this observation is different from that made in the ASH/ASI cilia of *C. elegans*, where the heterotrimeric kinesin-II failed to localize in the distal portions (Snow *et al.*, 2004).

To understand whether the continuous localization of KLP64D in the cilia indicates a role of the protein at the initiation of cilia assembly, we overexpressed the *UAS-KLP64D:GFP* transgene in two different *DmKap* hemizygous backgrounds where cilia growths are blocked in more than 80% ORNs. Surprisingly, this overexpression restored the initial phase of the cilia growth on the ORNs, innervating both *s. basiconica* and *s. trichodea* (Figure 7, A and B) in the mutants (Table 2). The cilia lengths recovered to the near wild-type levels (Figure 7E), and the volumes were restored to ~25% of the wild-type levels (Figure 7F). In addition, the EAG responses were restored to a similar extent in both the *DmKap* mutants (Figure 7G). This observation supported the argument that KLP64D indeed plays a vital role during procilium growth. In comparison, the expression of UAS-KLP68D:YFP in the *DmKap* mutants did not rescue the defects to the equivalent extent (Figure 7G, Table 2), indicating that either KLP68D is redundant in this process or relative levels of KLP64D and DmKAP are critical for kinesin-II functions in vivo.

KLP64D orthologues MmKif3A and Ceklp11 move processively in a heterodimer form in association with MmKif3B and Ceklp20, respectively (Muthukrishnan *et al.*, 2009; Brunnbauer *et al.*, 2010). In addition, a recent experiment in the laboratory showed that KLP64D stalk is unstable but folds into a stable heterodimer with KLP68D stalk in vitro in the absence of DmKAP (Doodhi *et al.*, 2009). Therefore, to localize into the cilia, KLP64D:GFP should associate with KLP68D or a similar motor subunit. The partial rescue due to the ectopic overexpression of KLP64D:GFP in the absence of DmKAP indicates that a motor subunit heterodimer containing KLP64D could partially substitute the heterotrimeric kinesin-II functions. It also indicates that DmKAP is needed to support the increased demand of kinesin-II activity during the second stage of the cilia growth and that the amount of KLP64D:GFP expression due to *Gal4^{chat19b}* is insufficient to supplement the loss of DmKAP entirely during this stage. The N-terminal fragment of DmKAP binds to the KLP64D/68D stalk heterodimer (Doodhi *et al.*, 2009). This binding is proposed to stabilize the KLP64D/68D heterotrimer. KLP64D stalk is unstable; it folds into a stable heterodimer in the presence of KLP68D in vitro (Doodhi, 2010). This result is similar to those obtained with Xklp3A and 3B (De Marco *et al.*, 2003). Therefore, KLP64D level in the cell is likely to control the rate of KLP64D/68D assembly in the absence of DmKAP. The lack of a significant partial rescue of the *DmKap* phenotypes due to the ectopic overexpression of KLP68D:YFP further supports this theory. Alternatively, KLP64D could associate with a different kinesin-II motor subunit with a functional overlap with KLP68D during the cilia assembly process. *Drosophila* genome analysis identified DmKif3C (CG17461; NP_661939.4) as a KLP64D and KLP68D homologue, but its function is unknown. Further experimental analysis will be needed to understand the exact molecular basis of this phenomenon and assign a clear role to the kinesin-II subunits in the process. Nevertheless, these results confirmed that heterotrimeric kinesin-II, consisting of KLP64D and DmKAP, plays a primary role in the cilia assembly process from the beginning.

Mutations in kinesin-II subunit genes affect tubulin localization into the cilia at multiple stages of development

Flagella and cilia contain distinct tubulin isoforms (Nielsen *et al.*, 2001). Mutations in certain α- (*tba-6 and tba-9*) and β-tubulin (*tbb-4*) genes disrupted cilia functions in *C. elegans* (Hurd *et al.*, 2010). In addition, the cilia MT subunits are multiply modified, viz., by acetylation, detyrosination, glutamylation, and so forth, which increase the MT stability (Lefebvre *et al.*, 1980; Libusova and Draber, 2006; McEwen *et al.*, 2007). We also noted that the expression of UAS-actin:GFP in the ORNs does not mark the cilia at any stage during

wild-type and mutant antennae used as benchmarks for the quantification: (a) branches containing singlet MT, (b) a branch containing multiple MTs, and (c) a lamella. (E) Histograms depict the distribution of different types of branches found in the OS of wild type and mutant basiconic shafts. Error bars represent ± standard deviation, and N ≥ 8, for all sets. (F) TEM images of the sections of *s. basiconica* from homozygous *DmKap^{v6}* adult antenna: (a) the cross-section view of a shaft and (b) the longitudinal section of an entire sensillum show the absence of cilia in the shaft. Scale bars indicate 50 nm for all images (D) and 500 nm for all images (C and F).

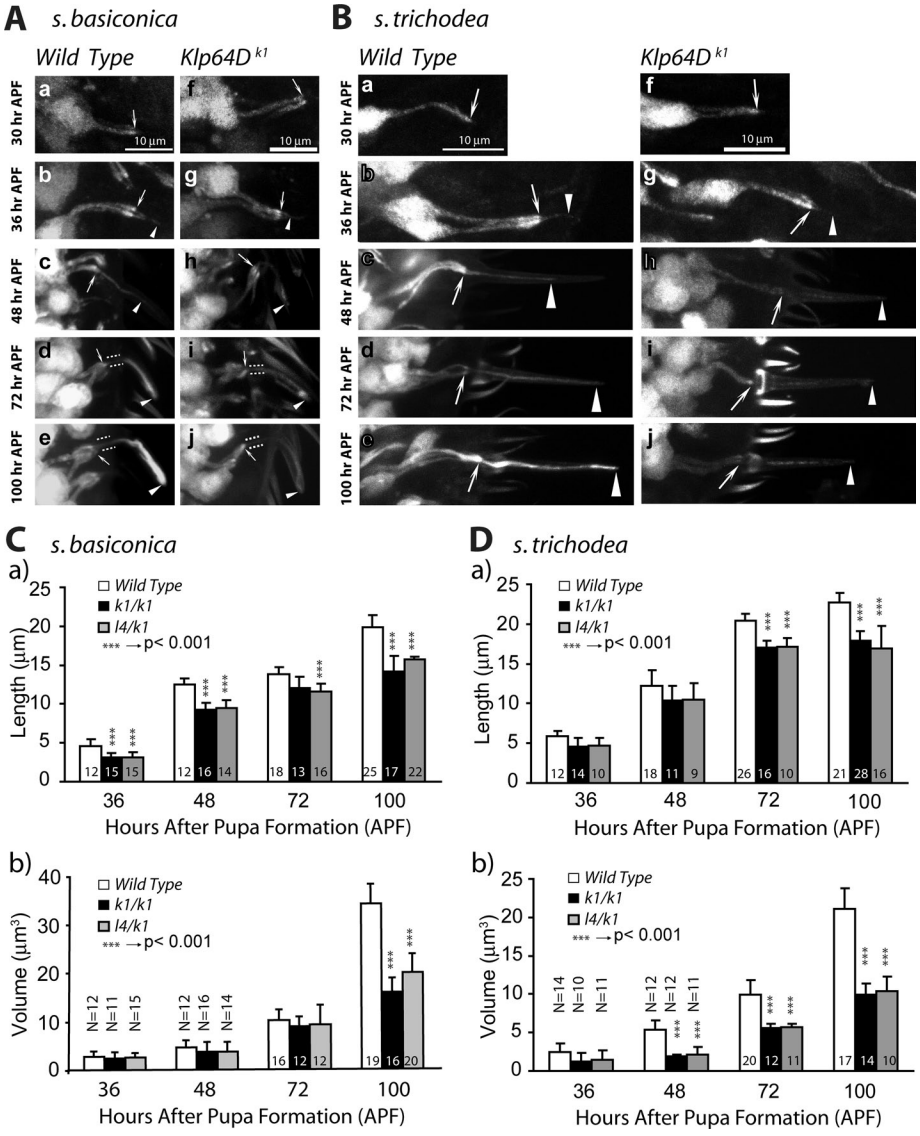

FIGURE 5: Cilia development defects in the *Klp64D* homozygous mutant antenna. (A and B) Stages of olfactory cilia growth inside *s. basiconica* (A) and *s. trichodea* (B) in the developing wild-type control (a–e) and *Klp64D*^{k1} (f–j) homozygous antennae. Arrows indicate the cilia base in the IS, paired dotted lines indicate the CC, and the arrowheads indicate the OS in each panel. Scale bar = 10 µm for all panels. (C and D) Histograms depict the temporal changes in the cilia lengths and volumes inside *s. basiconica* (C) and *s. trichodea* (D) in wild type and *Klp64D*^{k1} homozygous antennae. Error bars represent ± standard deviation, and the sample sizes (N values) are indicated on each bar. The pair-wise significance of the difference between the appropriate pair of wild-type and mutant data is tested by Student's *t* test, and highly significant differences ($p < 0.001$) are depicted by *** on the bars.

development (Supplemental Figure 4). Therefore the tubulin entry into the cilia is expected to promote its growth. We found that the acetylated α-tubulin is enriched in the IS and the ciliary OS regions in wild-type antennae (Figure 8, A–C and G–I). The staining appeared after 48-h APF (unpublished data), and its intensity as well as the stained area inside the shaft increased from 72 h APF onward (Figure 8, A–C and G–I). Thus acetylated α-tubulin staining provided a good marker for assessing MT stability in the cilia. As expected, the staining is visibly reduced and shortened in the homozygous *Klp64D*^{k1} (Figure 8, D and J) at 72 h APF, and failed to increase afterward (Figure 8, E, F, K, and L). A similar result was obtained in the homozygous *Klp68D*^{KG03849} antennae, but it was totally absent in the *DmKap* homozygous mutants (Supplemental Figure 5). Therefore the reduction or the total loss in acetylated α-tubulin staining as observed in the kinesin-II mutants could be caused by either reduced tubulin transport into the cilia or a block in MT acetylation.

To test the above conjectures, we expressed the *UAS-tubulin84B:GFP* in the ORNs, which was reported to mark other sensory cilia in *Drosophila* earlier (Avidor-Reiss *et al.*, 2004). In the *UAS-tubulin84B:GFP Gal4*^{cha19b}/+ antennae, some of the olfactory cilia were weakly labeled from 48 h APF (Figure 9, A and J), which then extended to the entire length of the cilia by 72 h APF (Figure 9, B and C), and both the volume as well as intensity of the fluorescence grew substantially until 100 h APF (Figure 9, K and L). This finding showed that the tubulin84B:GFP is selectively enriched in the ciliary OS as it develops. The localization, however, was visibly reduced in the *Klp64D*^{k1} (Figure 9, D–F and M–O) and disappeared in the *DmKap*^{v6} (Figure 9, G–I and P–R) homozygous backgrounds. The intensity of the tubulin84B:GFP fluorescence was visibly higher in the IS (Figure 9G) and the cell bodies (dashed line, Figure 9H) of the ORNs in the *DmKap*^{v6} antennae as compared with the wild-type, indicating that the absence of DmKAP blocks the ciliary entry of tubulin. In addition, the reduced level of tubulin in the ciliary OS in *Klp64D* mutants further suggests that kinesin-II is also required for tubulin entry during the second stage of OS growth. Although an exact correlation between the kinesin-II function and tubulin entry into the cilia is unclear, our data suggest that heterotrimeric kinesin-II is essential for tubulin entry into the cilia during development

DISCUSSION

We started the investigation with an aim to determine the roles of kinesin-II motors in generating the ciliary diversity in *Drosophila*. Results described earlier in text show that distinct patterns of growth underlie the diversity in the olfactory cilia. In addition, the heterotrimeric kinesin-II motor functions are required for propelling the cilia growth from the beginning. Our observations are in agreement with the results obtained from studies in the flagella (Kozminski *et al.*, 1995; Mueller *et al.*, 2005) and primary cilia as reviewed before (Silverman and Leroux, 2009). An earlier study also reported loss of olfactory cilia in the *nompB* mutants, which code for the IFT88 protein in *Drosophila* (Han *et al.*, 2003). Therefore, like the AWB cilia in *C. elegans* (Evans *et al.*, 2006; Mukhopadhyay *et al.*, 2007), the olfactory cilia in *Drosophila* also seem to grow in an IFT-dependent manner. Previous studies also indicated that the sensory cilia containing 9+0 axoneme are maintained by kinesin-II (Sarpal *et al.*, 2003) and IFT88 (Han *et al.*, 2003) and that KLP64D, along with some OSEG family of proteins, is involved in maintaining the mechanosensory cilia (Avidor-Reiss *et al.*,

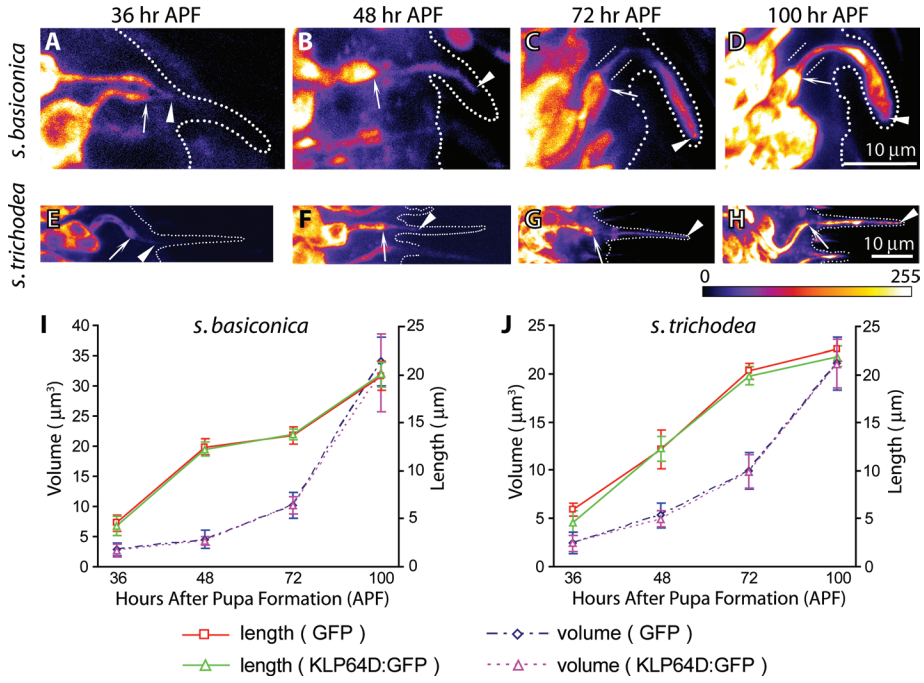

FIGURE 6: Recombinant KLP64D:GFP localizes in the growing ciliary OSs during development. (A–H) The *UAS-KLP64D:GFP* expression due to *Gal4*^{cha19B} highlighted the developing cilia on ORNs innervating the *s. basiconica* (A–D) and *s. trichodea* (E–H) at different stages of development as indicated on the top panel. Arrowheads mark the OS, and arrows indicate the IS in each figure. The broken line in each figure marks cuticle boundary as observed by simultaneous differential interference contrast (DIC) imaging of the specimen. Figures A–D are presented in the same scale as indicated on D, and the scale for E–H is indicated on H. The images are presented in an 8-bit color map as depicted below panel H to highlight the KLP64D:GFP localization in the developing cilia at early stages. (I–J) Line plots indicate the growth of cilia volume and length highlighted by KLP64D:GFP and GFP localizations in the cilia. Different colors are used to mark the length and volume profiles and distinguish between the values measured by KLP64D:GFP and GFP, respectively. Error bars represent ± standard deviation, and N ≥ 10 for all data points. The GFP data are presented as a reference. Note that the growth profiles measured by the KLP64D:GFP localization matched that of GFP indicating that KLP64D:GFP localizes into the cilia from the beginning.

2004). Together with the results presented here, these findings unified the role of kinesin-II as an essential motor for all bipartite sensory cilia assembly in *Drosophila*.

Our study also helped to establish that the heterotrimeric kinesin-II functions are essential for the olfactory cilia assembly from the beginning. The sensory cilia phenotypes of kinesin-II subunit mutants were mainly studied at the adult stages in *C. elegans* (Evans *et al.*, 2006; Mukhopadhyay *et al.*, 2008) and in the developed forms of zebra fish (Insinna *et al.*, 2008) and mice photoreceptor cells (Avasthi *et al.*, 2009). In these paradigms, it is difficult to distinguish their effects in the assembly and maintenance. The slow growth of the olfactory cilia allows studying the two processes separately. The data presented here established a detailed description of the growth of two morphologically different olfactory cilia during development. They showed that the process is extremely slow and occurs over several days. Moreover, the growth of basiconic cilium, which contains a branched OS, occurs in two stages with a short pause in between, whereas the trichoid cilium bearing a slender OS seems to grow in one single phase. In the absence of any other molecular characterization of the cilia growth process, it will be difficult to explain the basis of the differential growth profiles associated with the basiconic and trichoid cilia. We noted, however, that the pattern of growth is correlated to the structural diversity of the two cilia.

Ciliary growth requires combined transport of membrane and cytoskeleton components (Silverman and Leroux, 2009), and a complete picture of the process is still unclear. Earlier studies indicated that the presence of the "ciliary necklace" could stop the flow from the plasma membrane (Gilula and Satir, 1972), and recent studies indicated that the ran-GTPase and Importin-β regulate the KIF17 entry to the organelle (Dishinger *et al.*, 2010). In addition, the IFT particles are shown to dock on the transition filament at the cilia base. This evidence indicates that both the membranous and the soluble components of cilia must be supplied in synchrony through an actively gated transport. The primary cilia assembly occurs in four stages, and IFT is implicated in the last elongation step (step 4) of this process (reviewed in Pedersen *et al.*, 2008). Our results only confirm a kinesin-II requirement for the equivalent step 4 in case of sensory cilia. The data presented here would suggest that at an initial stage kinesin-II may facilitate tubulin or MT entry into the cilia to stabilize the initial growth. This suggestion is supported by the observation that null mutations in *DmKap* block tubulin entry from the beginning in a majority of the ORNs. In addition, kinesin-II is also required for tubulin entry during the second phase of OS growth as hypomorphic mutations in *Klp64D* also block tubulin entry as well as cilia growth after the procilia formation. There is a possibility that tubulin monomers may diffuse into the cilia and polymerize into MT in a kinesin-II–dependent manner. This possibility is highly unlikely because we monitored the tubulin localization by using tubulin84B:GFP, and somewhat indirectly, the MT assembly by acetylated α-tubulin staining in the mutant backgrounds. Both sets of data are consistent and indicate that kinesin-II functions are essential for tubulin entry. It is unclear whether this initiation process would require IFT.

We also found that the cilia growth is completed before the OR gene expressions in ORNs. In *Drosophila*, the olfactory cilia are present even though odor reception is entirely abolished in the *OR83b* mutants (Benton *et al.*, 2006). Previous results in *C. elegans* also indicated that, although the sensory inputs are required to maintain specialized architecture of AWB cilia, they are not essential for the cilia assembly (Mukhopadhyay *et al.*, 2008). Several transcription factors, however, appeared essential for maintaining the ciliary diversity (Mukhopadhyay *et al.*, 2007; Silverman and Leroux, 2009). Therefore, one can suggest that the cilia structure diversity is defined independent of sensory inputs and that the motor-based transport profiles are regulated by its intracellular environment. There is a possibility that the diversity in the cilia structure could be generated by differential transports of ciliary components, specifically tubulin subunits or MTs, by the heterotrimeric kinesin-II whereas the functional diversity could be achieved by transports due to accessory motors such as KIF17/Osm-3 in the olfactory cilia. Results discussed here helped to define a paradigm to further test these possibilities in *Drosophila*.

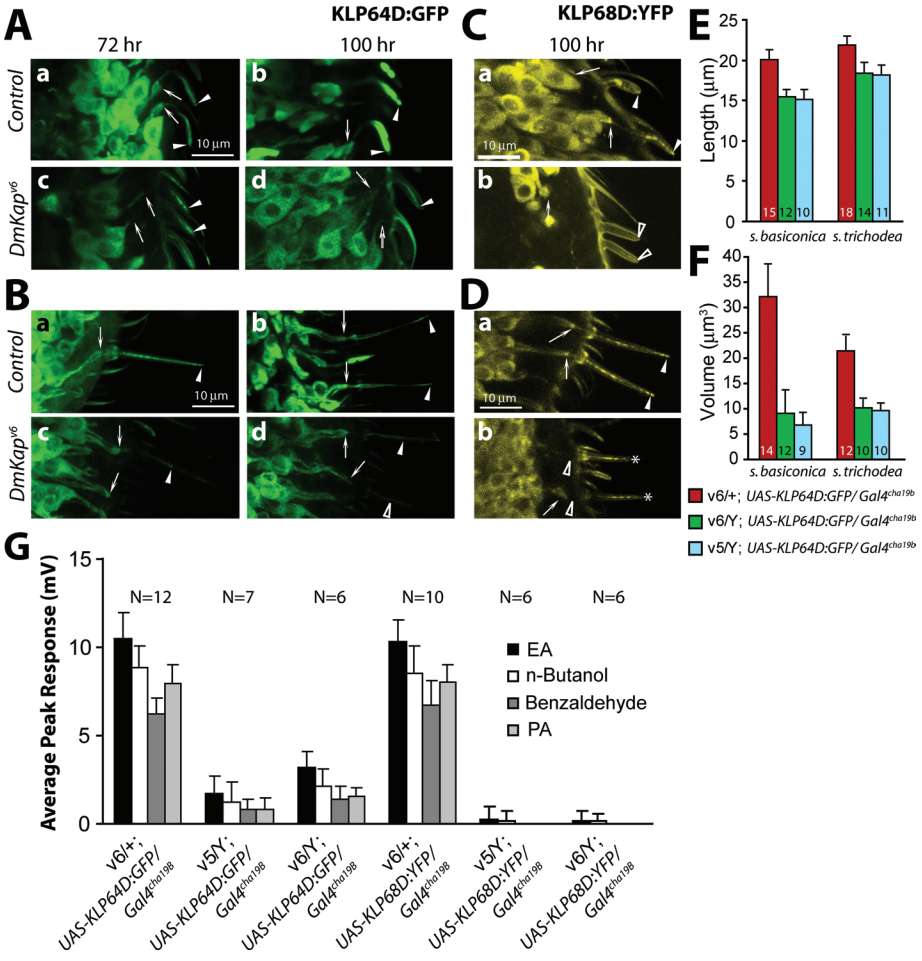

FIGURE 7: KLP64D overexpression in ORNs rescues the cilia growth defects in *DmKap* homozygous mutant background. (A and B) *UAS-KLP64D:GFP* is expressed in the ORNs innervating *s. basiconica* (A) and *s. trichodea* (B), respectively, by *Gal4*^{cha19b} in the *DmKap*^{v6}/+ as wild-type control (a and b) and *DmKap*^{v6} hemizygous (c and d) backgrounds for monitoring KLP64D:GFP localization and the cilia growth from ORNs. The localization was monitored at 72 h (a and c) and 100 h (b and d). (C and D) A similar experiment, done by expressing *UAS-KLP68D:YFP* in the ORNs innervating *s. basiconica* (C) and *s. trichodea* (D), respectively, in the wild-type control (a and b) and *DmKap*^{v6} hemizygous (c and d) backgrounds. The localization was only monitored at 100 h APF. Arrows in the figure indicate the cilia base, and arrowheads indicate the OS. The open arrows and arrowheads are used to indicate either thin or barely visible OS inside the shafts. All figures are shown in the same scale as shown by bars in subfigure (a) in all the figure sets. The rescue, due to the expression of *UAS-KLP68D:YFP*, was insignificant across all odors. (E and F) Histograms depict the cilia length (E) and volume (F) measured in wild-type controls and the *DmKap* hemizygous mutant backgrounds expressing *UAS-KLP64D:GFP*. The error bars indicate ± standard deviation, and the N values are indicated on each bar. The colors indicate different genotypes as indicated at the bottom. (G) Histograms show EAG responses of wild-type controls and *DmKap* hemizygous mutants, expressing either *UAS-KLP64D:GFP* or *UAS-KLP68D:YFP* in the ORNs, elicited by four different odors as indicated on the figure. The error bars indicate ± standard deviation, and the N values are indicated on the top of each set of bars. The responses to different odors are clustered together according to the genotype, as indicated below the horizontal margin. Note that *UAS-KLP64D:GFP* expression partly rescued the total loss of EAG observed in the *DmKap* mutants earlier.

MATERIALS AND METHODS

Fly stocks

Fly stocks used in this study are described in Supplemental Table 1 and listed in the "FlyBase" (www.flybase.org). *Klp64D*, *Klp68D*, and *DmKap* code for the heterotrimeric kinesin-II subunits in *Drosophila*. *Klp64D*^{k1} bears a nonsense (UAA) mutation at the 13th residue in the predicted KLP64D ORF (Ray *et al.*, 1999). The homozygous *Klp64D*^{k1} flies were severely uncoordinated and mostly failed to emerge from the pupae. Contrary to the current belief, an ongoing genetic analysis in the laboratory suggests that *Klp64D*^{k1} is strongly hypomorphic and survives to the adult stage (K. Ray, unpublished data). *Klp64D*^{l4} carries G102D mutation in the motor domain (Sarpal *et al.*, 2003), and it is the strongest lethal allele in our collection. *Klp64D*^{l4} homozygous animals die in the third instar larva or early pupa stages. We have used different combinations of *Klp64D* alleles to determine the role of KLP64D in olfactory cilia development. *Klp68D*^{KG03849} and *Klp68D*^{EY00199}, generated by the Gene Disruption Project consortia (Bellen *et al.*, 2004), were obtained from the FlyBase (www.flybase.org). Both of these alleles were reported to contain a P-element insertion at the 5′ untranslated region of KLP68D. The homozygous adults are viable and fertile. The *DmKap*^{v5} and *DmKap*^{v6} are the strongest alleles of the gene with no detectable protein expression in the tissue (S. C. Jana and K. Ray, unpublished data). Few homozygous *DmKap*^{v5} and *DmKap*^{v6} animals develop to pharate adults, and even fewer emerge from the pupae. The emerged flies are severely uncoordinated. The *UAS-Klp64D* (Ray *et al.*, 1999) and *UAS-DmKap* (Sarpal *et al.*, 2003) constructs were previously reported. The *UAS-Klp64D:GFP* and *UAS-Klp68D:YFP* transgenes were constructed by separately subcloning the Klp64D and Klp68D complementary DNA fragments into the NotI/KpnI sites of pP{UAS-T} vector with the *GFP* and *YFP*, respectively, inserted at the 3′ ends between the *Kpn*I and *Xba*I sites. The fusion constructs were transformed by using standard techniques to obtain stable stocks.

EAG recording

EAGs were recorded using saline-filled capillary glass electrodes from 1- to 2-d-old adult flies as described earlier (Alcorta, 1991). The recording electrode was placed on the *s. basiconica*–rich region of the third antennal segment, and the ground electrode was inserted into the head capsule. For each trial, air puffs saturated with odorants [diluted in paraffin oil, 1/10,000 (vol/vol)] were delivered to the mounted fly heads for 0.5 s using an electromechanical device, and responses obtained from three consecutive trials were averaged for one data point. The instrumentation and data acquisition software were developed in-house using standard amplifiers and LabView (National Instruments, Austin, TX) programming interface. Several different recessive lethal alleles of *Klp64D* (*viz.*, *k1*, *k5*, and *l4*) and *DmKap* (*viz.*, *v6* and *v5*) and two different P-element insertion alleles of *Klp68D* (viz., *KG03849* and *EY00199*) were used for this screen by exposing them to four different odor pulses (*viz.*, ethyl acetate, n-butanol, benzaldehyde, and propionic acid). The first three odors are sensed by *s. basiconica*

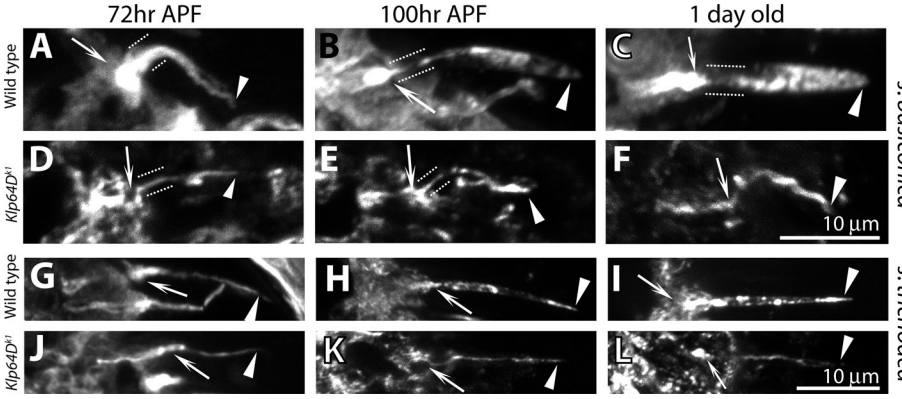

FIGURE 8: Mutations in *Klp64D* reduce tubulin acetylation in the ciliary OSs. Anti–acetylated α-tubulin staining highlighted the IS (arrows) and the entire olfactory cilia (arrowheads) in the wild type (A–C and G–I) and homozygous *Klp64D*^{k1} (D–F and J–L) adults. Panels A–F show staining in *s. basiconica,* and G–L show staining in *s. trichodea*. Arrowhead indicates the OS, paired dotted lines mark the CC region, and arrow indicate the IS in each panel. The pictures were taken from antennal sections at 72 h (A, D, G, and J) and 100 h (B, E, H, and K) and from 1-d-old adults (C, F, I, and L). A–F and G–H are shown in the same scale as indicated by the bars (10 µm each) in F and L, respectively.

(Goldman *et al.*, 2005), whereas both the n-butanol as well as propionic acid are sensed by *s. coeloconica* (Yao *et al.*, 2005).

Electron microscopy

Dissected fly heads carrying intact antennae were fixed and processed as described (Sarpal *et al.*, 2003). Serial 50-nm sections of the tissue blocks were obtained in a Leica Ultracut UC6 (Leica Microsystems, Wetzlar, Germany) using a diamond knife (Diatome 45), collected on a formvar-coated copper slot and examined in a Zeiss Libra 120 EFTEM (Carl ZEISS-SMT, Oberkochen, Germany). The images were collected by using a bottom-mounted 2k×2k-TRS slow-scan CCD camera and further processed in Photoshop (Adobe Systems, San Jose, CA) for presentation.

Immunostaining, fluorescence image acquisition, and processing

For the cilia development study, third antennal segments of 30- to 100-h-APF pupae expressing *UAS-eGFP* were dissected in phosphate-buffered saline (PBS), 137 mM NaCl, 2.7 mM KCl, 10 mM Na_2HPO_4, 1.76 mM KH_2PO_4 and pH 7.4; fixed in 4% formaldehyde solution (4% paraformaldehyde in PBS, pH 7.4) for 30 min at room temperature; and, after a quick rinse in PBS, mounted in Vectashield (Vector Laboratories, Burlingame, CA) on a glass slide under a 0.17-mm glass coverslip. The preparations were then imaged using a confocal microscope (Olympus FV1000SPD; Olympus Imaging Corp., Tokyo, Japan) as described later in the text. To monitor the intracellular distribution of fluorescently tagged kinesin-II subunits and tubulin84B:GFP in the tissue, the third antennal segments from 30- to 100-h-APF pupae, expressing *UAS-Klp64D:GFP*, *UAS-tubulin84B:GFP*, and so forth, were dissected in PBS and further processed as detailed earlier in the text. To study the localization of acetylated α-tubulin, *Drosophila* heads were dissected, sectioned in a cryomicrotome (Leica), and fixed following a standardized protocol (Dobritsa *et al.*, 2003). Ribbons of ~10 µm tissue sections obtained from the cryomicrotome were laid on a poly-D-lysine–coated slide and fixed in 4% formaldehyde solution for 30 min at room temperature. Then they were stained with a 1:500 dilution of monoclonal antibody–acetylated α-tubulin (Sigma, St. Louis, MO) in blocking solution and Alexafluor647-conjugated goat anti–mouse (Molecular Probes, Eugene, OR) secondary antibody, according to a published method (Dobritsa *et al.*, 2003). Finally, they were mounted in Vectashield (Vector Laboratories) for microscopic examination

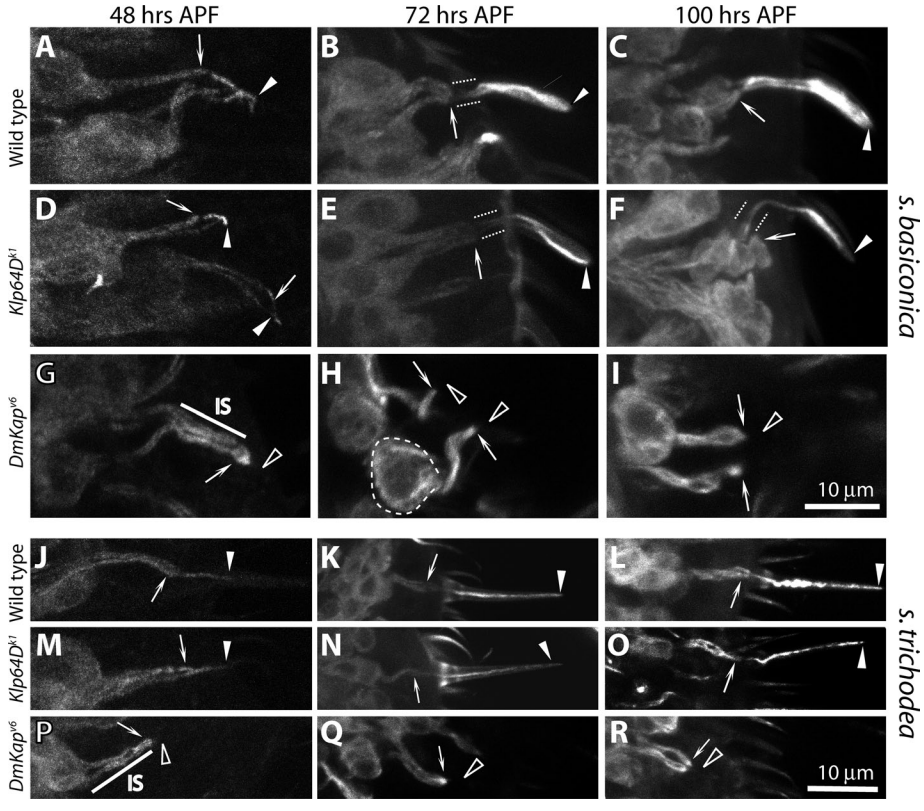

FIGURE 9: The tubulin84B::GFP localization in the developing olfactory cilia. The *UAS-tubulin84B::GFP* expression in the ORNs due to *Gal4*^{cha19b} in the wild-type (A–C and J–L), homozygous *Klp64D*^{k1} (D–F and M–O), and *DmKap*^{v6} (G–I and P–R) backgrounds highlighted the developing cilia on the ORNs innervating *s. basiconica* (A–F) and *s. trichodea* (G–L) from 48 h APF onward, whereas *UAS-eGFP* expression due to the same driver marked the cilia from 36 h APF (Supplementary Figure 1A). Arrowheads indicate the OS, paired dotted lines mark the CC region, and arrows indicate the cilia base in each panel. A–I and J–R are shown in the same relative scales as indicated by the bars in I and R, respectively, both of which indicate 10 µm.

as described earlier in the text. All fluorescence microscopy images were collected under comparable conditions using the Olympus FV1000SPD confocal microscope equipped with a 63× 1.4 NA objective lens (Olympus Imaging Corp., Tokyo, Japan). Cilia length and volumes were measured after a three-dimensional rendering of the selected image stacks by using the Imaris 6.1.5 graphics package (Bitplane Scientific Solutions, Zurich, Switzerland). Subsequently, all images were processed using ImageJ (rsweb.nih.gov/IJ) and Photoshop (Adobe) following identical steps. All figures containing images and line art were composed in Illustrator (Adobe) and converted to TIFF format before uploading.

ACKNOWLEDGMENTS

The project was supported by an intramural grant from the Tata Institute of Fundamental Research, Department of Atomic Energy, to KR. We sincerely acknowledge the help and support provided by S. Shirolikar and L. Borde of the Cryo-TEM facility of TIFR for the TEM data, B. Karmakar for setting up the EAG apparatus, R. Phadke and K. Bobra for help, M. Narasimhan for generously supply of antibody, and Mr. Gajendra of Kushal Biosciences, India, for preparing the transgenic flies. We also thank members of the KR's laboratory for patient reading of the draft manuscript.

REFERENCES

Alcorta E (1991). Characterization of the electroantennogram in Drosophila melanogaster and its use for identifying olfactory capture and transduction mutants. J Neurophysiol 65, 702–714.

Arikawa K, Williams DS (1989). Organization of actin filaments and immunocolocalization of alpha-actinin in the connecting cilium of rat photoreceptors. J Comp Neurol 288, 640–646.

Avasthi P, Watt CB, Williams DS, Le YZ, Li S, Chen CK, Marc RE, Frederick JM, Baehr W (2009). Trafficking of membrane proteins to cone but not rod outer segments is dependent on heterotrimeric kinesin-II. J Neurosci 29, 14287–14298.

Avidor-Reiss T, Maer AM, Koundakjian E, Polyanovsky A, Keil T, Subramaniam S, Zuker CS (2004). Decoding cilia function: defining specialized genes required for compartmentalized cilia biogenesis. Cell 117, 527–539.

Bellen HJ *et al*. (2004). The BDGP gene disruption project: single transposon insertions associated with 40% of Drosophila genes. Genetics 167, 761–781.

Benton R, Sachse S, Michnick SW, Vosshall LB (2006). Atypical membrane topology and heteromeric function of Drosophila odorant receptors in vivo. PLoS Biol 4, e20.

Brunnbauer M, Mueller-Planitz F, Kosem S, Ho TH, Dombi R, Gebhardt JC, Rief M, Okten Z (2010). Regulation of a heterodimeric kinesin-2 through an unprocessive motor domain that is turned processive by its partner. Proc Natl Acad Sci USA 107, 10460–10465.

Burns RG (1979). Kinetics of the regeneration of sea-urchin cilia. II. Regeneration of animalized cilia. J Cell Sci 37, 205–215.

Chaitin MH (1991). Actin filaments in the photoreceptor cilium of the rds mutant mouse. Exp Eye Res 53, 107–113.

Chizhikov VV, Davenport J, Zhang Q, Shih EK, Cabello OA, Fuchs JL, Yoder BK, Millen KJ (2007). Cilia proteins control cerebellar morphogenesis by promoting expansion of the granule progenitor pool. J Neurosci 27, 9780–9789.

Clyne P, Grant A, O'Connell R, Carlson JR (1997). Odorant response of individual sensilla on the Drosophila antenna. Invert Neurosci 3, 127–135.

Cole DG, Chinn SW, Wedaman KP, Hall K, Vuong T, Scholey JM (1993). Novel heterotrimeric kinesin-related protein purified from sea urchin eggs. Nature 366, 268–270.

Corbit KC, Aanstad P, Singla V, Norman AR, Stainier DY, Reiter JF (2005). Vertebrate Smoothened functions at the primary cilium. Nature 437, 1018–1021.

Davenport JR, Watts AJ, Roper VC, Croyle MJ, van Groen T, Wyss JM, Nagy TR, Kesterson RA, Yoder BK (2007). Disruption of intraflagellar transport in adult mice leads to obesity and slow-onset cystic kidney disease. Curr Biol 17, 1586–1594.

Davenport JR, Yoder BK (2005). An incredible decade for the primary cilium: a look at a once-forgotten organelle. Am J Physiol Renal Physiol 289, F1159–F1169.

de Bruyne M, Foster K, Carlson JR (2001). Odor coding in the Drosophila antenna. Neuron 30, 537–552.

De Marco V, De Marco A, Goldie KN, Correia JJ, Hoenger A (2003). Dimerization properties of a Xenopus laevis kinesin-II carboxy-terminal stalk fragment. EMBO Rep 4, 717–722.

Dishinger JF, Kee HL, Jenkins PM, Fan S, Hurd TW, Hammond JW, Truong YN, Margolis B, Martens JR, Verhey KJ (2010). Ciliary entry of the kinesin-2 motor KIF17 is regulated by importin-beta2 and RanGTP. Nat Cell Biol 12, 703–710.

Dobritsa AA, Van Der Goes van Naters W, Warr CG, Steinbrecht RA, Carlson JR (2003). Integrating the molecular and cellular basis of odor coding in the Drosophila antenna. Neuron 37, 827–841.

Doodhi H (2010). Mechanism of kinesin-2 assembly in Drosophila melanogaster: in vitro analysis of domain-wise interaction amongst the subunits, Tata Institute of Fundamental Research, Mumbai, India.

Doodhi H, Ghosal D, Krishnamurthy M, Jana SC, Shamala D, Bhaduri A, Sowdhamini R, Ray K (2009). KAP, the accessory subunit of kinesin-2, binds the predicted coiled-coil stalk of the motor subunits. Biochemistry 48, 2248–2260.

Evans JE, Snow JJ, Gunnarson AL, Ou G, Stahlberg H, McDonald KL, Scholey JM (2006). Functional modulation of IFT kinesins extends the sensory repertoire of ciliated neurons in Caenorhabditis elegans. J Cell Biol 172, 663–669.

Gilula NB, Satir P (1972). The ciliary necklaceA ciliary membrane specialization. J Cell Biol 53, 494–509.

Goetz SC, Anderson KV (2010). The primary cilium: a signalling centre during vertebrate development. Nat Rev Genet 11, 331–344.

Goldman AL, Van Der Goes van Naters W, Lessing D, Warr CG, Carlson JR (2005). Coexpression of two functional odor receptors in one neuron. Neuron 45, 661–666.

Han YG, Kwok BH, Kernan MJ (2003). Intraflagellar transport is required in Drosophila to differentiate sensory cilia but not sperm. Curr Biol 13, 1679–1686.

Hirokawa N, Tanaka Y, Okada Y, Takeda S (2006). Nodal flow and the generation of left-right asymmetry. Cell 125, 33–45.

Hurd DD, Miller RM, Nunez L, Portman DS (2010). Specific alpha- and beta-tubulin isotypes optimize the functions of sensory Cilia in Caenorhabditis elegans. Genetics 185, 883–896.

Insinna C, Pathak N, Perkins B, Drummond I, Besharse JC (2008). The homodimeric kinesin, Kif17, is essential for vertebrate photoreceptor sensory outer segment development. Dev Biol 316, 160–170.

Jaffe LF (2007). Stretch-activated calcium channels relay fast calcium waves propagated by calcium-induced calcium influx. Biol Cell 99, 175–184.

Jenkins PM, Hurd TW, Zhang L, McEwen DP, Brown RL, Margolis B, Verhey KJ, Martens JR (2006). Ciliary targeting of olfactory CNG channels requires the CNGB1b subunit and the kinesin-2 motor protein, KIF17. Curr Biol 16, 1211–1216.

Kozminski KG, Beech PL, Rosenbaum JL (1995). The Chlamydomonas kinesin-like protein FLA10 is involved in motility associated with the flagellar membrane. J Cell Biol 131, 1517–1527.

Larsson MC, Domingos AI, Jones WD, Chiappe ME, Amrein H, Vosshall LB (2004). Or83b encodes a broadly expressed odorant receptor essential for Drosophila olfaction. Neuron 43, 703–714.

Lefebvre PA, Nordstrom SA, Moulder JE, Rosenbaum JL (1978). Flagellar elongation and shortening in Chlamydomonas. IV. Effects of flagellar detachment, regeneration, and resorption on the induction of flagellar protein synthesis. J Cell Biol 78, 8–27.

Lefebvre PA, Rosenbaum JL (1986). Regulation of the synthesis and assembly of ciliary and flagellar proteins during regeneration. Annu Rev Cell Biol 2, 517–546.

Lefebvre PA, Silflow CD, Wieben ED, Rosenbaum JL (1980). Increased levels of mRNAs for tubulin and other flagellar proteins after amputation or shortening of Chlamydomonas flagella. Cell 20, 469–477.

Libusova L, Draber P (2006). Multiple tubulin forms in ciliated protozoan Tetrahymena and Paramecium species. Protoplasma 227, 65–76.

Loktev AV, Zhang Q, Beck JS, Searby CC, Scheetz TE, Bazan JF, Slusarski DC, Sheffield VC, Jackson PK, Nachury MV (2008). A BBSome subunit links ciliogenesis, microtubule stability, and acetylation. Dev Cell 15, 854–865.

McEwen DP, Koenekoop RK, Khanna H, Jenkins PM, Lopez I, Swaroop A, Martens JR (2007). Hypomorphic CEP290/NPHP6 mutations result in anosmia caused by the selective loss of G proteins in cilia of olfactory sensory neurons. Proc Natl Acad Sci USA 104, 15917–15922.

Mesland DA, Hoffman JL, Caligor E, Goodenough UW (1980). Flagellar tip activation stimulated by membrane adhesions in Chlamydomonas gametes. J Cell Biol 84, 599–617.
Morris RL, Scholey JM (1997). Heterotrimeric kinesin-II is required for the assembly of motile 9+2 ciliary axonemes on sea urchin embryos. J Cell Biol 138, 1009–1022.
Mueller J, Perrone CA, Bower R, Cole DG, Porter ME (2005). The FLA3 KAP subunit is required for localization of kinesin-2 to the site of flagellar assembly and processive anterograde intraflagellar transport. Mol Biol Cell 16, 1341–1354.
Mukhopadhyay S, Lu Y, Qin H, Lanjuin A, Shaham S, Sengupta P (2007). Distinct IFT mechanisms contribute to the generation of ciliary structural diversity in C. elegans. EMBO J 26, 2966–2980.
Mukhopadhyay S, Lu Y, Shaham S, Sengupta P (2008). Sensory signaling-dependent remodeling of olfactory cilia architecture in C. elegans. Dev Cell 14, 762–774.
Muthukrishnan G, Zhang Y, Shastry S, Hancock WO (2009). The processivity of kinesin-2 motors suggests diminished front-head gating. Curr Biol 19, 442–447.
Nielsen MG, Turner FR, Hutchens JA, Raff EC (2001). Axoneme-specific beta-tubulin specialization: a conserved C-terminal motif specifies the central pair. Curr Biol 11, 529–533.
Ou G, Qin H, Rosenbaum JL, Scholey JM (2005). The PKD protein qilin undergoes intraflagellar transport. Curr Biol 15, R410–R411.
Pan J, Snell WJ (2002). Kinesin-II is required for flagellar sensory transduction during fertilization in Chlamydomonas. Mol Biol Cell 13, 1417–1426.
Pan X, Ou G, Civelekoglu-Scholey G, Blacque OE, Endres NF, Tao L, Mogilner A, Leroux MR, Vale RD, Scholey JM (2006). Mechanism of transport of IFT particles in Celegans cilia by the concerted action of kinesin-II and OSM-3 motors. J Cell Biol 174, 1035–1045.
Pedersen LB, Geimer S, Rosenbaum JL (2006). Dissecting the molecular mechanisms of intraflagellar transport in chlamydomonas. Curr Biol 16, 450–459.
Pedersen LB, Veland IR, Schroder JM, Christensen ST (2008). Assembly of primary cilia. Dev Dyn 237, 1993–2006.
Praetorius HA, Spring KR (2001). Bending the MDCK cell primary cilium increases intracellular calcium. J Membr Biol 184, 71–79.
Ray K, Perez SE, Yang Z, Xu J, Ritchings BW, Steller H, Goldstein LS (1999). Kinesin-II is required for axonal transport of choline acetyltransferase in Drosophila. J Cell Biol 147, 507–518.
Reese TS (1965). Olfactory cilia in the frog. J Cell Biol 25, 209–230.
Sarpal R, Todi SV, Sivan-Loukianova E, Shirolikar S, Subramanian N, Raff EC, Erickson JW, Ray K, Eberl DF (2003). Drosophila KAP interacts with the kinesin II motor subunit KLP64D to assemble chordotonal sensory cilia, but not sperm tails. Curr Biol 13, 1687–1696.
Scholey JM (2003). Intraflagellar transport. Annu Rev Cell Dev Biol 19, 423–443.
Shah AS *et al*. (2008). Loss of Bardet-Biedl syndrome proteins alters the morphology and function of motile cilia in airway epithelia. Proc Natl Acad Sci USA 105, 3380–3385.
Shanbhag SR, Muller B, Steinbrecht RA (1999). Atlas of olfactory organs of Drosophila melanogaster: 1. Types, external organization, innervation and distribution of olfactory sensilla. Int J Insect Morphol Embryol 28, 377–397.
Silverman MA, Leroux MR (2009). Intraflagellar transport and the generation of dynamic, structurally and functionally diverse cilia. Trends Cell Biol 19, 306–316.
Singla V, Reiter JF (2006). The primary cilium as the cell's antenna: signaling at a sensory organelle. Science 313, 629–633.
Snow JJ, Ou G, Gunnarson AL, Walker MR, Zhou HM, Brust-Mascher I, Scholey JM (2004). Two anterograde intraflagellar transport motors cooperate to build sensory cilia on C. elegans neurons. Nat Cell Biol 6, 1109–1113.
Van Der Goes van Naters W, Carlson JR (2007). Receptors and neurons for fly odors in Drosophila. Curr Biol 17, 606–612.
Wang Q, Pan J, Snell WJ (2006). Intraflagellar transport particles participate directly in cilium-generated signaling in Chlamydomonas. Cell 125, 549–562.
Ward S, Thomson N, White JG, Brenner S (1975). Electron microscopical reconstruction of the anterior sensory anatomy of the nematode Caenorhabditis elegans. J Comp Neurol 160, 313–337.
Wong SY, Seol AD, So PL, Ermilov AN, Bichakjian CK, Epstein EH Jr, Dlugosz AA, Reiter JF (2009). Primary cilia can both mediate and suppress Hedgehog pathway-dependent tumorigenesis. Nat Med 15, 1055–1061.
Yao CA, Ignell R, Carlson JR (2005). Chemosensory coding by neurons in the coeloconic sensilla of the Drosophila antenna. J Neurosci 25, 8359–8367.
Yoder BK, Hou X, Guay-Woodford LM (2002). The polycystic kidney disease proteins, polycystin-1, polycystin-2, polaris, and cystin, are co-localized in renal cilia. J Am Soc Nephrol 13, 2508–2516.

ETOC:

Structurally distinct sensory cilia in the fly antenna grow in different stepwise patterns. The heterotrimeric kinesin-II is essential for growth at all stages, and it is also required for tubulin entry into the cilia from the beginning. This report establishes a primary function of the motor in the bipartite cilia assembly in *Drosophila*.